

Long-range convective ozone transport during INTEX

M. L. B ker,¹ Matthew H. Hitchman,¹ Gregory J. Tripoli,¹ R. B. Pierce,² E. V. Browell,² and J. A. Al-Saadi²

Received 1 September 2007; revised 11 February 2008; accepted 21 March 2008; published 18 July 2008.

[1] Ozone transport across the tropopause near a convective region in the central Pacific is calculated for a 1-day period using a nested grid, high-resolution simulation with the University of Wisconsin Nonhydrostatic Modeling System (UWNMS). This ozone is then tracked into the region where DC-8 lidar ozone observations on 6 July 2004 were taken over the United States during the Intercontinental Chemical Transport Experiment-North America (INTEX-NA). On 2 July a convective complex developed north of the Midway Islands and intensified as it propagated eastward. Satellite observations captured this event well, and the UWNMS simulation placed the convection just east of an upper level trough along the subtropical jet. The proximity of the strong convection to the lowered tropopause resulted in significant stratospheric ozone contribution (SOC) to the troposphere. During the 24 h period starting at 1200 UTC 2 July, total net ozone flux into the troposphere was calculated to be about 0.2 Tg across the nested grid domain. Because the convective outflow was feeding the subtropical jet, the SOC was quickly transported across the eastern Pacific and into the INTEX-NA region. Using an ‘‘SOC tracer’’ we show that a small but significant percentage of observed ozone on the DC8 flight can be attributed to SOC from this one convective event. This supports the idea that the stratosphere over the Pacific is an important source of ozone for air entering North America from the west.

Citation: B ker, M. L., M. H. Hitchman, G. J. Tripoli, R. B. Pierce, E. V. Browell, and J. A. Al-Saadi (2008), Long-range convective ozone transport during INTEX, *J. Geophys. Res.*, 113, D14S90, doi:10.1029/2007JD009345.

1. Introduction

[2] One of the primary goals of the Intercontinental Chemical Transport Experiment-North America (INTEX-NA) was to quantify transpacific transport of ozone from anthropogenic sources in east Asia and the stratospheric ozone contribution (SOC) over the Pacific and their impact on tropospheric ozone over North America [Singh *et al.*, 2006]. The INTEX-NA campaign was conducted during 1 July to 15 August 2004.

[3] The onset of the summer monsoon over the western North Pacific (150 to 180 W) begins in July [e.g., Wu and Wang, 2000], increasing low-level moisture convergence over the region. When an upper level trough (or jet streak) moves into this environment, mesoscale convective system (MCS) formation can occur [e.g., Waugh and Funatsu, 2003] (hereinafter referred to as WF2003). These convective events have been shown to be a significant source of SOC to the troposphere as a result of downwelling around the periphery of the convection [Poulida *et al.*, 1996; Hitchman *et al.*, 2004]. The MCS which began to form

on 2 July developed near an upper level trough, just southwest of a jet streak. The University of Wisconsin Nonhydrostatic Modeling System (UWNMS) was used to simulate this convection and its effect on ozone redistribution. A schematic diagram of this process is shown in Figure 1.

[4] In addition, the outflow from the convection led to enhancement of the jet streak [e.g., Fritsch and Maddox, 1981; Mecikalski and Tripoli, 1998, 2003], creating a conduit for long-range transport of SOC over North America. Four days later, INTEX DC-8 ozone observations on flight 4 surveyed a portion of the southwestern United States, where a small, yet significant percentage of background tropospheric ozone could be attributed to the SOC by the convective event.

[5] This paper presents a case study yielding quantification of the SOC in the convective region. It also provides quantification of SOC transported into the INTEX-NA region.

[6] Coincident studies involving SOC include Al-Saadi *et al.* [2005] (hereinafter referred to as AS2005), who examined the time mean impact of SOC (among other constituents and sources) over the INTEX domain using Lagrangian source-receptor analysis, and found midlatitude upper tropospheric air had a significant source region in the central Pacific lower stratosphere. Pierce *et al.* [2007] calculated SOC using a discrete method with the Realtime Air Quality Modeling System (RAQMS) in the context of a continental ozone budget

¹Department of Atmospheric Sciences, University of Wisconsin-Madison, Madison, Wisconsin, USA.

²NASA Langley Research Center, Hampton, Virginia, USA.

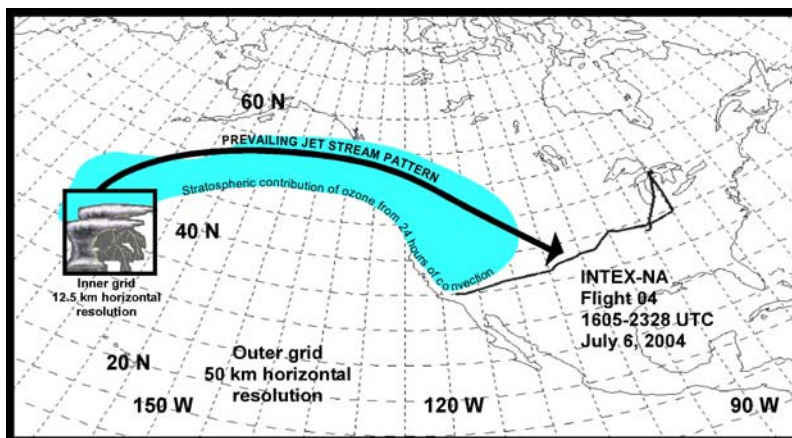


Figure 1. Schematic showing the domains of the inner and outer nested grid, horizontal path of INTEX-NA flight 4, and a general overview of the convectively induced long-range SOC transport process.

over North America. Since these analyses look at SOC over the period of several weeks, they include various modes of SOC, including synoptic-scale events as tropopause folding and Rossby wave breaking, as well as mesoscale events such as convective complexes. A discussion comparing our local processes with their bulk results is made in section 4.2. Many studies have aimed to quantify SOC in the vicinity of synoptic-scale disturbances [e.g., Wirth and Egger, 1999; Wei, 1987; Ebel *et al.*, 1991; Lamarque and Hess, 1994; Sigmond *et al.*, 2000; Gray, 2003]. Büker *et al.* [2005] applied a new two-scale method toward calculating SOC in the vicinity of a strongly filamented jet and strengthening cyclone.

[7] Hitchman *et al.* [2004] (hereinafter referred to as H2004) utilized this technique for a large convective event over east Asia, and found that about 0.8 Tg d^{-1} of ozone entered the troposphere around the periphery of the convection. Given the frequency of convective events over the central Pacific (WF2003), it is desirable to examine the ozone flux around a convective complex in the context of long-range transport of SOC.

[8] A description of the UWNMS and model specifications are provided in section 2, followed by details of the two-scale method and SOC tracer, and an overview of aircraft and satellite data used in this study. Section 3 gives an asymptotic overview of the case study for both the convective region and the far-field domain along with UWNMS simulation results. Section 4 describes INTEX-NA DC-8 flight 4 observations and compares them with our results. A summary of the results is given in section 5.

2. Model and Observational Data

2.1. UWNMS Specifications and Initialization

[9] The UWNMS is a multiscale numerical weather prediction model, applicable physics scalable to processes on scales ranging from meters to typical general circulation model resolutions [Tripoli, 1992] along with two-way, interactive multiple nested grid capabilities. The model has a history of utilization in recent field campaigns such as the SAGE III Ozone Loss and Validation Experiment (SOLVE), and Transport and Chemical Evolution over the Pacific (TRACE-P) campaigns [Hitchman *et al.*, 1999, 2003, 2004]. The UWNMS has also been combined with

a global isentropic model [Johnson *et al.*, 1993] and a detailed chemistry package from the Langley IMPACT model [Eckman *et al.*, 1995] to create the Regional Air Quality Modeling System (RAQMS) [Pierce *et al.*, 2003].

[10] We initialize the meteorological fields with Global Forecast System (GFS) analyses from the National Center for Environmental Prediction with $1^\circ \times 1^\circ$ horizontal resolution, interpolated to a model grid with isotropic horizontal resolution of 50 km. This large outer grid spanned much of the central and eastern North Pacific region and North America, centered at 125°W and 45°N , with the domain extending 11,000 km zonally and 7,000 km meridionally. Additionally, for a 1-day period, a nested, two-way interactive grid with 12.5 km horizontal resolution was placed at 35°N and 168°W , spanning 1,250 km on each side. Figure 1 shows the horizontal extent of both the inner and outer grids. Vertical resolution was kept constant for all simulations at 300 m, with the top of the domain extending to 22.5 km. Rayleigh friction sponge layers were implemented on the sidewalls (7 grid points) and top (10 grid points) of each domain. The UWNMS has several convective parameterizations that can be used; we have chosen the Emanuel moist convection scheme for consistency with other RAQMS studies. Three dimensional ozone profiles of the same resolution as the GFS data are obtained from RAQMS simulations [Pierce *et al.*, 2007] and allowed to advect as a passive tracer. After initialization, the boundary conditions are forced by subsequent analyses, linearly interpolated in time and space with updates every 6 h, while the interior is allowed to evolve within the parameters of the model physics. Standard meteorological fields (e.g., winds, temperature, pressure, water vapor, rainfall) as well as derived and constituent fields (e.g., potential vorticity and ozone) are archived at 20 and 30 min intervals in VIS-5D format [Hibbard *et al.*, 1994], with the simulations spanning 5 days. The model time step for the outer grid was 60 s, and 15 s for the inner grid.

2.2. Two-Scale Method and SOC Tracer

[11] Mass flux across the tropopause is calculated using the two-scale method described by Büker *et al.* [2005], with some minor modification. A range of PV values spans the upper troposphere and lower stratosphere. The 1.3 potential

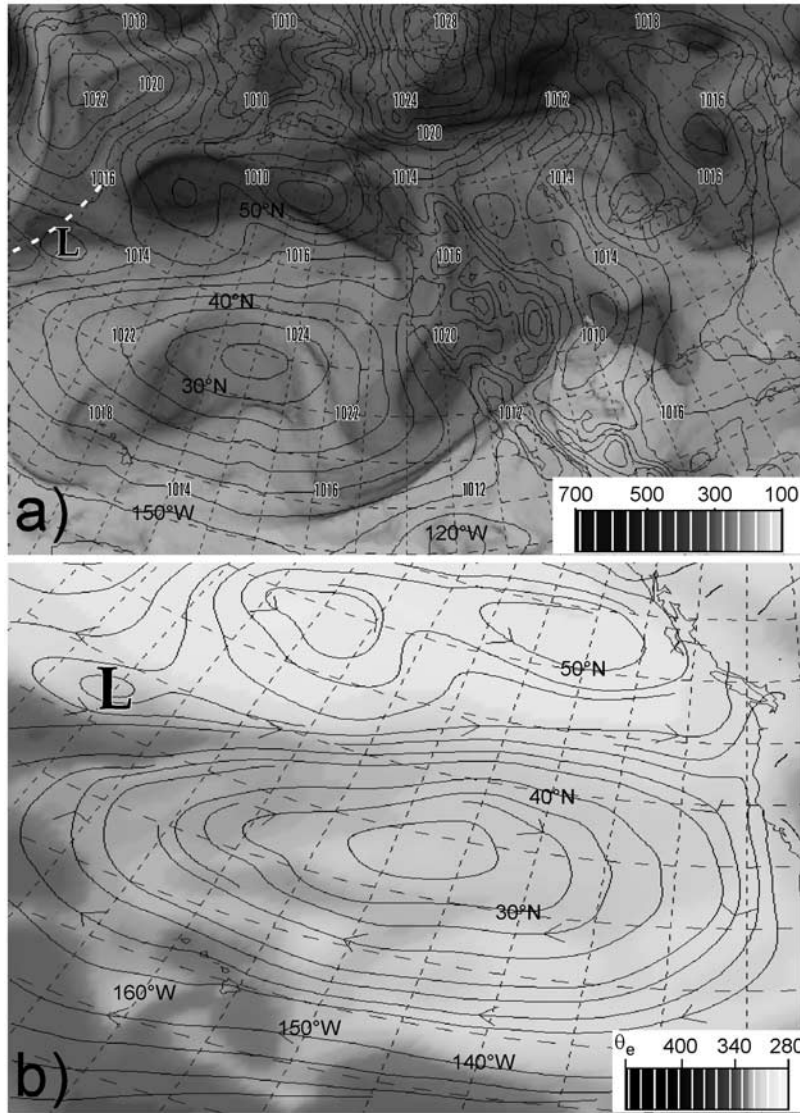


Figure 2. (a) Structure of the tropopause (1.3 PVU surface) at 1200 UTC 2 July 2004. The surface is shaded by pressure (hPa), where darker indicates a lower altitude. Sea level pressure (black contours, every 2 hPa) is also indicated. Note the surface trough (denoted with an “L”) and upper level shortwave (white dashed line) around 37°N and 175°W. (b) Horizontal streamlines and equivalent potential temperature (K) at 1 km altitude for the same time, showing surface convergence and a plume of moisture in the vicinity of the surface low.

vorticity unit (PVU) surface is used for this study. The low-pass filter used to separate the wind field into the advective, conserving flow (\mathbf{V}_s) and smaller-scale (resolved) nonconservative “mixing” motions ($\mathbf{V}_m = \mathbf{V} - \mathbf{V}_s$) is now based on the modified Barnes scheme [Barnes, 1973]. The response of this filter [Maddox, 1980] is given by

$$R = R_0 \left(1 + R_0^{g-1} - R_0^g \right),$$

where

$$R_0 = \exp(-\pi^2 4c/\lambda^2).$$

The parameters c and g are chosen to tune the filter, and λ is the wavelength. With $c = 30000$ and $g = 0.1$, the filter retains 90% of the wind field at 1000 km, 60% at 500 km, and 25% at 300 km scales. As opposed to the 1-2-1 “triangle filter” used by Bükler, et al. [2005] (where hundreds of passes are needed at high resolution and large spatial scales [Haltiner and Williams, 1980]), only two passes are required for tuning the filter to the correct spatial scale. Additionally, the dropoff in the response function is much sharper around horizontal scales of 300–500 km, which was shown to be an ideal separation scale [Bükler et al., 2005]. The PV tropopause is calculated and advected using this smoothed wind field, with its motion described by $(\mathbf{V}_s \cdot \mathbf{n})\mathbf{n}$, with \mathbf{n} the local vector norm of the tropopause surface. Flux is then assigned the value of the mixing wind

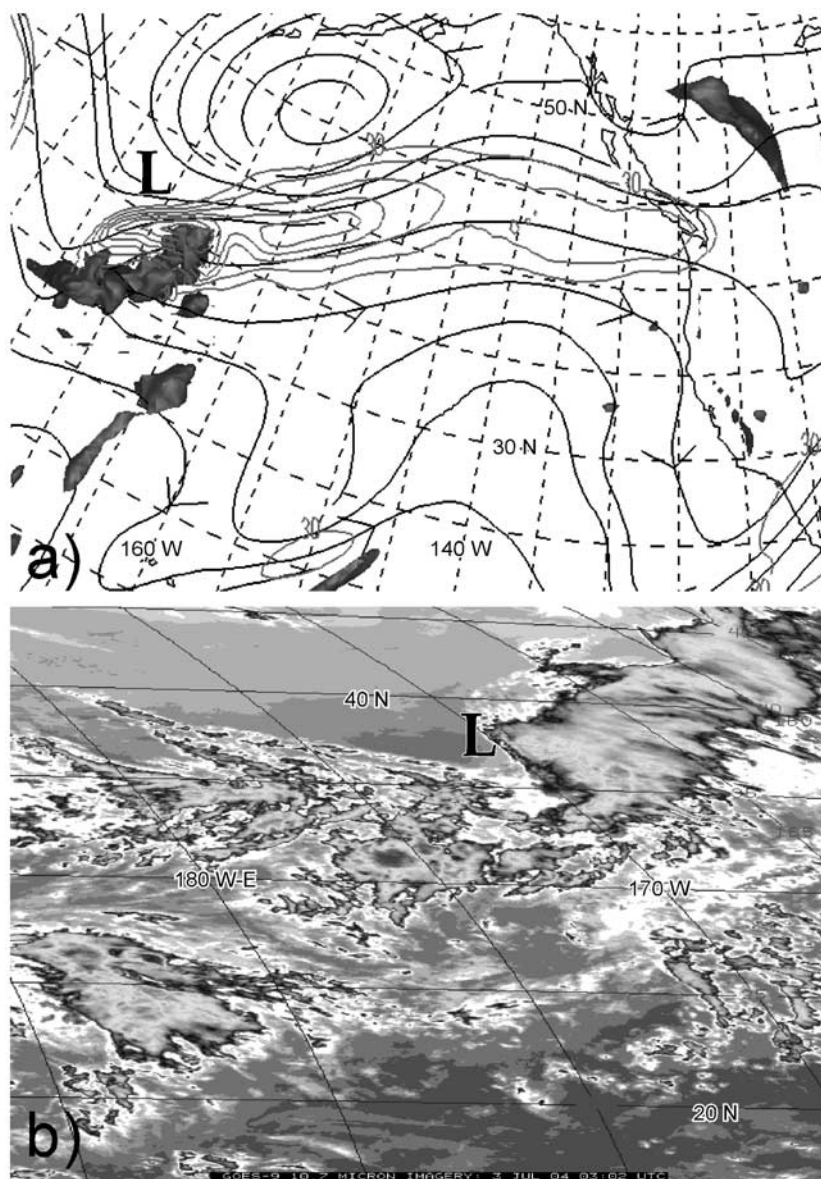


Figure 3. (a) Vertical motion (0.1 m s^{-1} isosurface, indicating convection in the UWNMS) and 11.5 km horizontal streamlines (black) and isotachs (grey, every 10 m s^{-1}) at 0000 UTC 3 July, showing the direction of the convective outflow. (b) A GOES 9 infrared image for 0302 UT 3 July, with an L indicating the position of the surface low and convection.

normal to the tropopause, or $\chi_{O_3}(\mathbf{V}_m \cdot \mathbf{n})\mathbf{n}$, where χ_{O_3} is the local ozone number density. The ozone field is left unaltered, retaining the small-scale variability of both the tracer and of \mathbf{V}_m to obtain the fine structure of the flux normal to the smoothed PV surface, circumventing uncertainty in gradient calculations of a noisy PV field, and providing an upper limit on the flux without resorting to uncertainties in real and numerical diffusion.

[12] Upon calculation of SOC using this method, a passive “SOC tracer” is increased or decreased in value according to the sign and magnitude of the instantaneous flux. Values can be added or subtracted to account for ozone transported both into and out of the stratosphere. As the flux was calculated and archived only every 20 min (because of computational expense), the value was multiplied by that

time interval. In terms of advection, diffusion, and other modes of transport, it is treated as any other passive tracer in the model. The tracer can accumulate in the inner grid, but is allowed to advect into the larger domain. This allows for direct attribution of SOC due to the convective region in the far-field.

[13] To more accurately simulate photochemical influences, ozone production and loss rates were calculated by the global isentropic and chemistry components of the RAQMS, interpolated to the outer grid and updated every 6 h.

2.3. Observational Data

[14] Water vapor imagery from GOES 9 and GOES 10 was provided by the Space Science and Engineering and the National Climate Data Center. Visible and infrared imagery

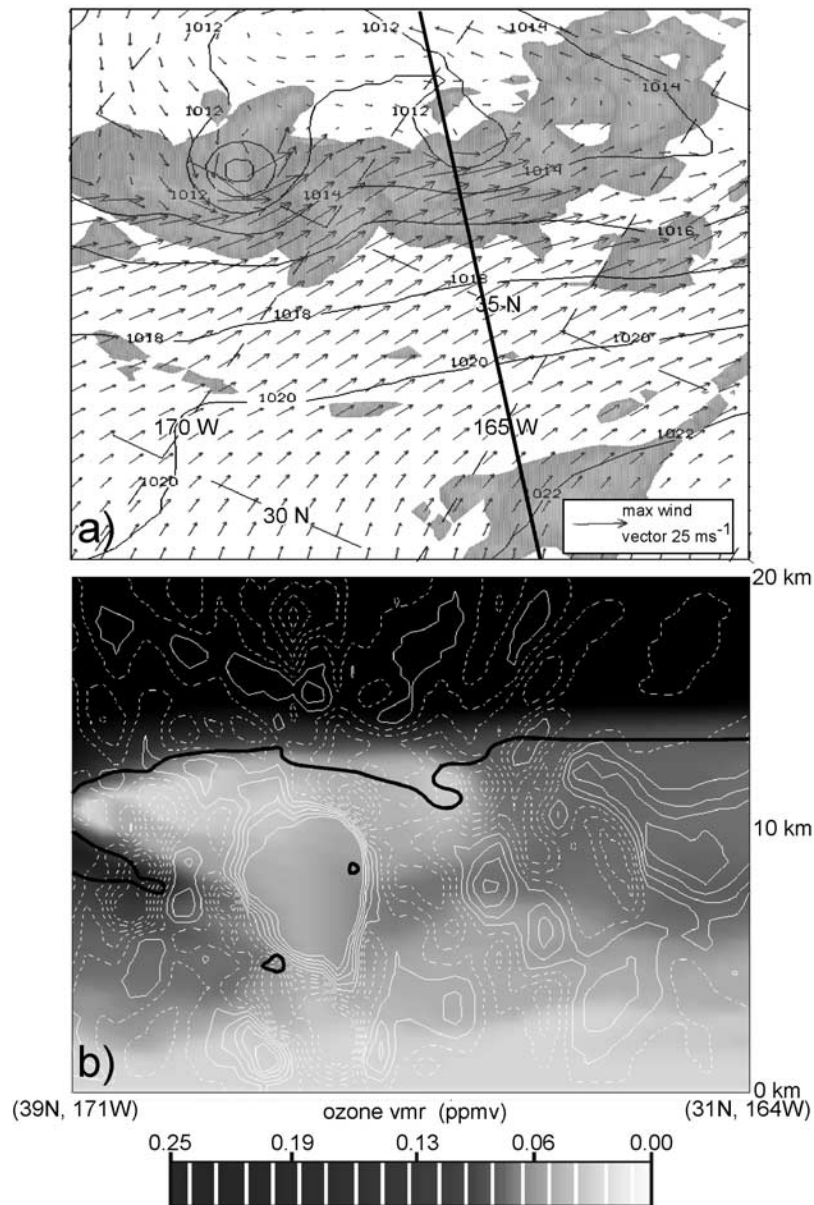


Figure 4. A view of convection in the inner grid at 0000 UT 3 July, showing (a) vertical motion exceeding 0.1 m s^{-1} , contours of sea level pressure (every 2 hPa), and surface wind vectors. (b) A northwest-southeast vertical cross section (position shown above) of ozone (ppmv, shaded), vertical motion (white contours, every 0.02 m s^{-1} , dashed for downward velocities), and the 1.3 PVU contour (black). Note the horizontal convergence in Figure 4a and “V-shaped” pattern of vertical velocity (indicating gravity waves) in Figure 4b.

from Japan’s Geostationary Meteorology Satellite 5 (GMS-5) were used to correlate synoptic and convective features in the simulations. Time-height profiles of Langley Differential Absorption Lidar (DIAL, see <http://asd-www.larc.nasa.gov/lidar/intex-na/dial/04.html>) ozone for DC-8 flight 4 are used to compare with ozone structure in the UWNMS.

3. Case Study for INTEX-NA Flight 4: 2–6 July 2004

3.1. Synoptic Overview, Convective Region: 2–3 July

[15] The UWNMS simulation was carried out in three stages. Only the outer grid (see section 2) was used for the

first 12 h from 0000 UTC to 1200 UTC 2 July. The inner grid was activated for the next 24 h of the simulation, until 1200 UTC 3 July. After this, only the outer grid was used for the remaining 84 h of integration, until 0000 UTC 7 July.

[16] Figure 2a shows mean sea level pressure and the 1.3 PVU isosurface shaded by pressure for 1200 UTC 2 July. The feature of interest is a compact shortwave, centered just west of surface low pressure (L) near 37°N , 175°W . This shortwave was traveling northeastward around a large upper ridge extending from 20 to 35°N and 160°W to the dateline. Figure 2b shows values of equivalent potential temperature

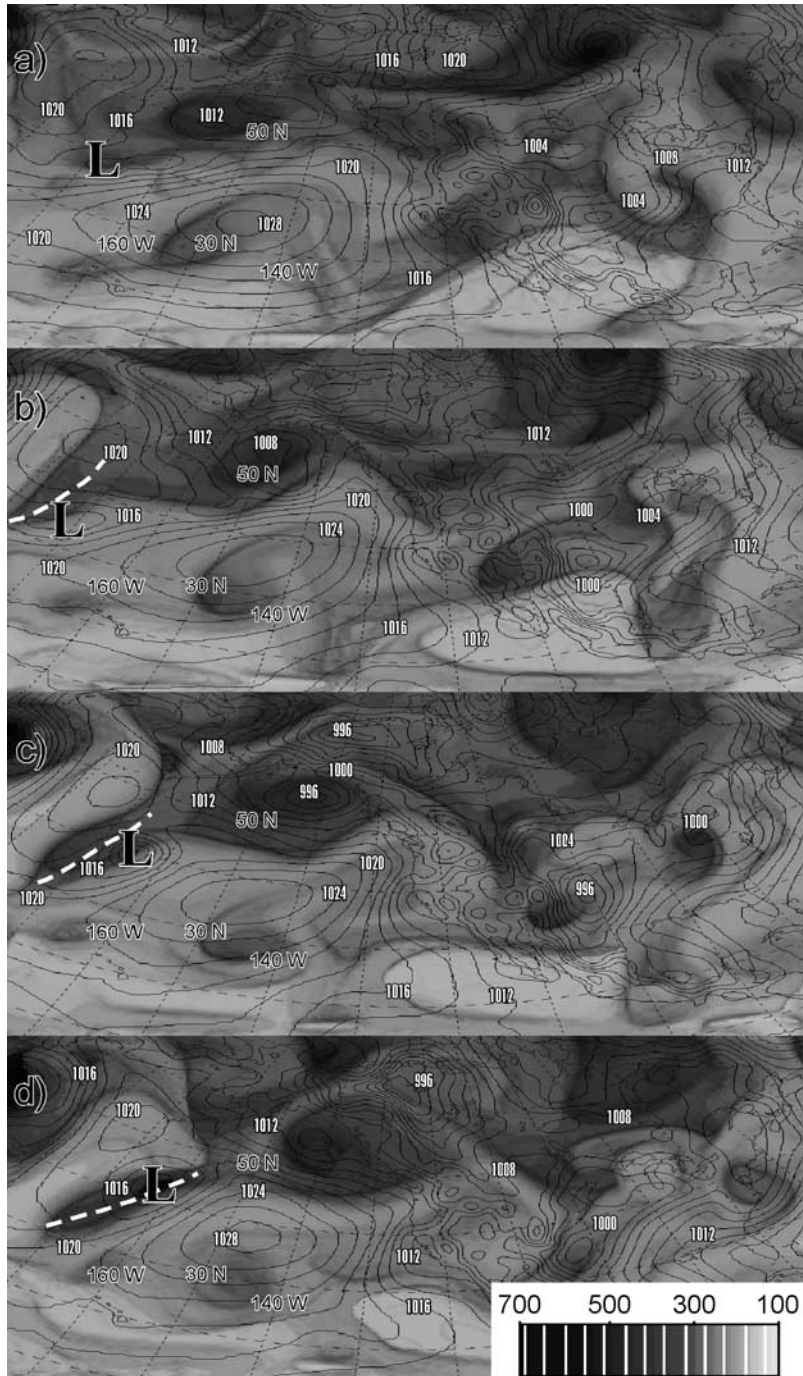


Figure 5. As in Figure 2a, at 1200 UT for (a) 3 July, (b) 4 July, (c) 5 July, and (d) 6 July, showing the large Rossby wave breaking (RWB) feature extending from the southwestern United States to north of Hawaii. The strong potential vorticity anomaly (and convectively enhanced ridge south of it) moves east across the Gulf of Alaska, disturbing the RWB signature and pushing the ridge over the western United States.

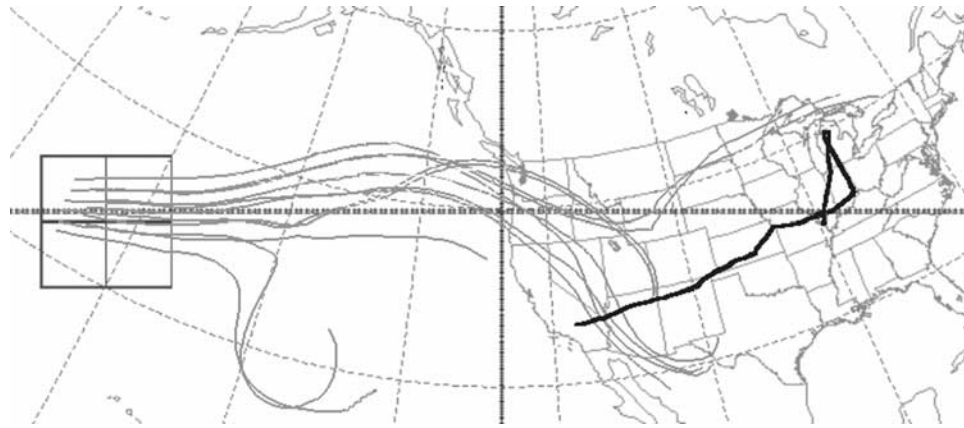


Figure 6. Four-day trajectories initialized 1200 UTC 3 July in the vicinity of the convection at 11.5 km. Note the split flow near the shortwave over the Rockies.

(θ_e) and horizontal streamlines at 1 km altitude for the same time period. Strong surface convergence can be seen in the vicinity of the shortwave. Southwesterly flow is bringing high θ_e air from a region where the monsoonal circulation becomes established during this time of year [Wu and Wang, 2000]. It is not surprising that convection developed in the region just east of the shortwave, given this combination of strong moisture convergence at low levels, pressure height falls and positive vorticity advection [Holton, 1992]. In addition, Figure 3 (top) reveals that this area should also experience enhanced ascent, as it underlies the right rear quadrant of a large jet streak (shaded regions) [Bluestein, 1993]. This collocation of a narrow stratospheric intrusion and transient convection occurs quite frequently over the central and eastern North Pacific, with static stability being reduced in the upper troposphere (WF2003). Upper tropospheric streamlines also show upper level divergence in this area, enhancing upward motion. The 0.1 m s^{-1} isosurface (dark “blobs”) shows where convection is being simulated.

[17] These storms organized into a multicellular squall line, as the 0–4 km wind shear (not shown) was fairly strong and unidirectional. GOES 9 Satellite imagery ($10.7 \mu\text{m}$ infrared) (Figure 3, bottom) for 0400 UTC 3 July shows a line of convection extending from 45°N , 155°W to 32°N , 170°W , which correlated very well with the UWNMS location for the convection. The convection had two effects on the jet: first, by acting as a solid body impinging from below, the jet was redirected northward. Second, by transporting westerly momentum further northward, the jet intensified on the northeastern flank of the convective complex. *Mecikalski and Tripoli* [1998] investigated this type of momentum transfer (conversion of “inertial available kinetic energy”) through convection. The intensified jet stream, collocated with convectively driven stratospheric downwelling, would provide an ideal conduit for long-range transport of SOC.

[18] Figure 4a shows the inner grid of the simulation, with sea level pressure, surface winds, and the 0.1 m s^{-1} isosurface of vertical motion on 0000 UT 3 July. The squall line was well developed by this point, with vertical velocities exceeding 2.5 m s^{-1} in the strongest cells. Strong convergence is noted in the surface wind field (arrows) along the axis of convection. On the periphery of the broader synoptic depression, a compact area of low pressure

is collocated with the strongest convection. Figure 4b is a vertical cross section of ozone mixing ratio, the 1.3 PVU contour, and vertical motion. Relatively high mixing ratio values are being brought down around the periphery of the convection (as evidenced by higher values of downward vertical velocities), while low tropospheric values are transported up through the convective turret [Poulida *et al.*, 1996]. H2004 examined a similar case study with dramatic downwelling (and associated SOC) surrounding a mesoscale convective system. Squall lines also tend to produce a broad spectrum of gravity and inertia-gravity waves [Alexander *et al.*, 1995] which can contribute to stratosphere-troposphere exchange (STE) through Stokes drift [Stokes, 1847]. and wave breaking. The vertical motion field shows the typical “V-shaped” structures in the stratosphere emanating from the top of the convection [Holton, 1992]. The close juxtaposition of the convective system with the lowered tropopause of the compact shortwave maximized the potential for STE in both directions. A 24-h integration was chosen to capture the bulk of this activity. Once SOC was produced in this region, the intensified jet transported it nearly a quarter of the way around the 45°N latitude circle.

3.2. Synoptic Overview, Long-Range Transport and Flight 4: 3–6 July

[19] The broader synoptic situation is depicted in Figure 5, with the pressure-shaded 1.3 PVU isosurface and mean sea level pressure contours for 3–6 July. A large reversal in the meridional PV gradient is evident throughout the sequence in varying intensity, stretching from the west coast of the United States to north of Hawaii. This is a signature of a Rossby wave breaking (RWB) event, a common occurrence in this region during boreal summer [Postel and Hitchman, 1999, 2001; Hitchman and Huesmann, 2007]. RWB occurs centered near 45°N , 135°W , with considerable mixing of tropical tropospheric and stratospheric air above the surface high. This is an example of an “LC1” equatorward wave-breaking event [Thorncroft *et al.*, 1993]. The convection associated with the shortwave, approaching from the west near 50°N , 155°W , further intensified the ridge (through the redistribution of lower tropospheric PV to higher altitudes by latent heating [Hoskins *et al.*, 1985]), thereby enhancing

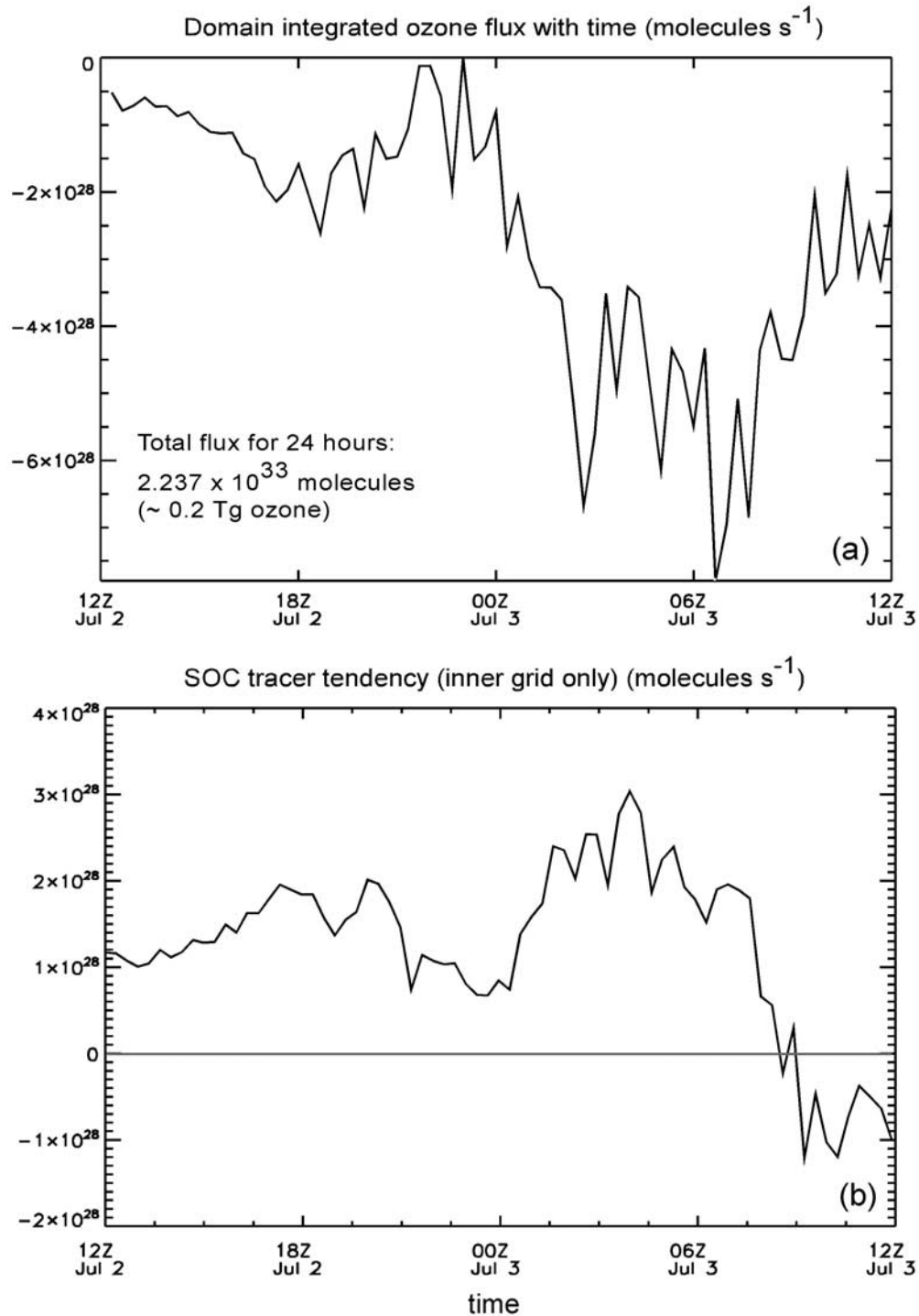


Figure 7. (a) Spatially integrated net ozone flux (SOC) with time for the inner grid (see Figure 1) from 1200 UTC 2 July to 1200 UTC 3 July. Negative values indicate flux into the troposphere. (b) Tendency of SOC tracer with time. Note the close agreement early in the period, with a decreasing trend in SOC for the inner grid as tracer leaves the domain.

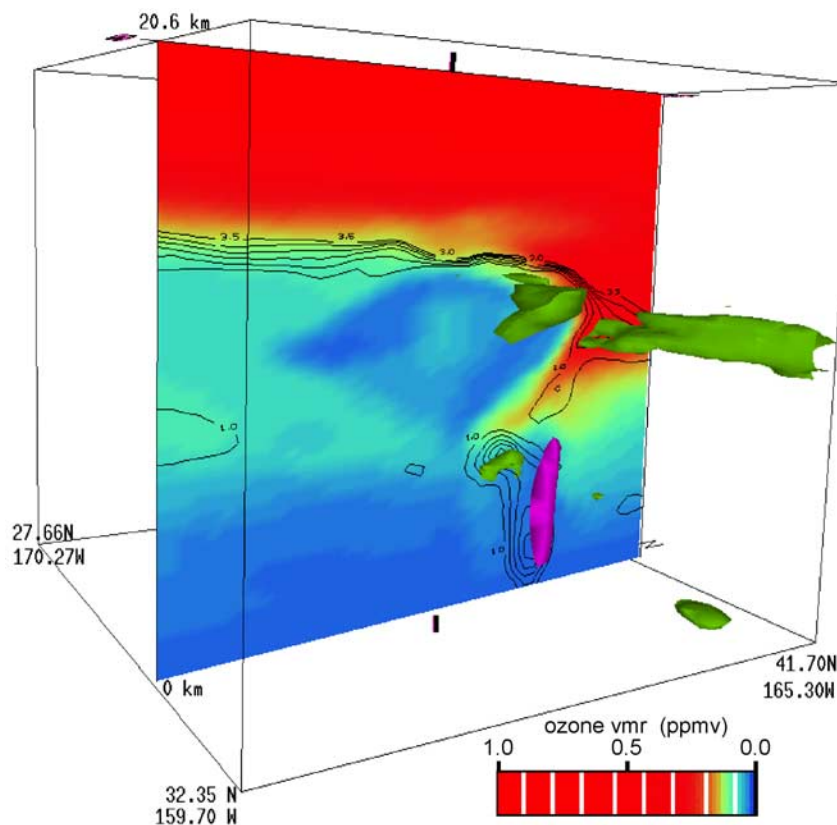


Figure 8. Vertical cross section of ozone (colored/shaded index, ppmv) and contours of potential vorticity (every 0.5 PVU) perpendicular to the line of convection in the inner grid at 0800 UTC 3 July. Isosurfaces of vertical motion (purple, 0.5 m s^{-1}), and SOC (green, values exceeding 40% of the background ozone) are also shown. Convective dilution of ozone is evident, while SOC is prevalent along the northern flank of the convection, above a small tropopause fold. A patch of new SOC is also generated where convection is impinging on the fold. Note that the SOC tracer indicates accumulated flux, not instantaneous values.

the meridional PV gradient (and the associated jet streak). Another shortwave anomaly near 50°N , 125°W traveled eastward, a feature encountered on INTEX flight 4 over the western United States.

[20] Figure 6 shows 4-day trajectories, initialized at 11.5 km (within the convective outflow) and the plan view of flight 4. The flow stays fairly contained within the jet stream, with a split occurring over the western United States. The majority of the trajectories end up over the southwestern United States by the time flight 4 commences. This provides a qualitative picture of the impact of STE and long-range transport on the beginning portion of the flight domain.

3.3. Ozone and SOC Analysis

3.3.1. Inner Grid: 2–3 July

[21] Total net flux of ozone over the inner grid was calculated for the 24-h period starting 1200 UTC 2 July. Negative flux indicates transfer down the PV gradient (into the troposphere) while positive flux indicates upgradient transfer. The domain integrated values are computed at each time and plotted in Figure 7a. This shows a maximum in net flux occurring between 0200 and 0800 UTC, which coincides with peak diurnal heating. The peak value of nearly -8×10^{28} ozone molecules s^{-1} is comparable to other

studies of STE and convective complexes [e.g., Poulida *et al.*, 1996; H2004]. Integrating over the 24 h, the total net flux out of the domain was 2.3×10^{33} molecules, or about 0.2 Tg ozone. H2004 estimated about 0.8 Tg of SOC associated with a larger convective complex for 1 day. Poulida *et al.* [1996] used aircraft observations to obtain a minimum of 0.02 Tg SOC around the periphery of an MCS in its developing stage, but for a shorter time. In addition to the strong downwelling around the convection, a strong PV anomaly was also situated along the northern flank of the convective area, with a structure resembling a small tropopause fold.

[22] Figure 8 shows a vertical-meridional cross section through the inner grid of ozone (colored slice), PV contours near the tropopause, and an isosurface of vertical motion (purple) exceeding 0.5 m s^{-1} at 0800 UTC 3 July, just after the period of the most vigorous convection. Ozone-poor air from the lower troposphere has been injected into the upper troposphere by the convection. Downwelling is apparent on the flanks of the convection, with high values reaching into the middle troposphere. On the northern flank, the downwelling appears to be coincident with a small tropopause fold (and high ozone values) extending into the middle troposphere. New convection is occurring in the simulation

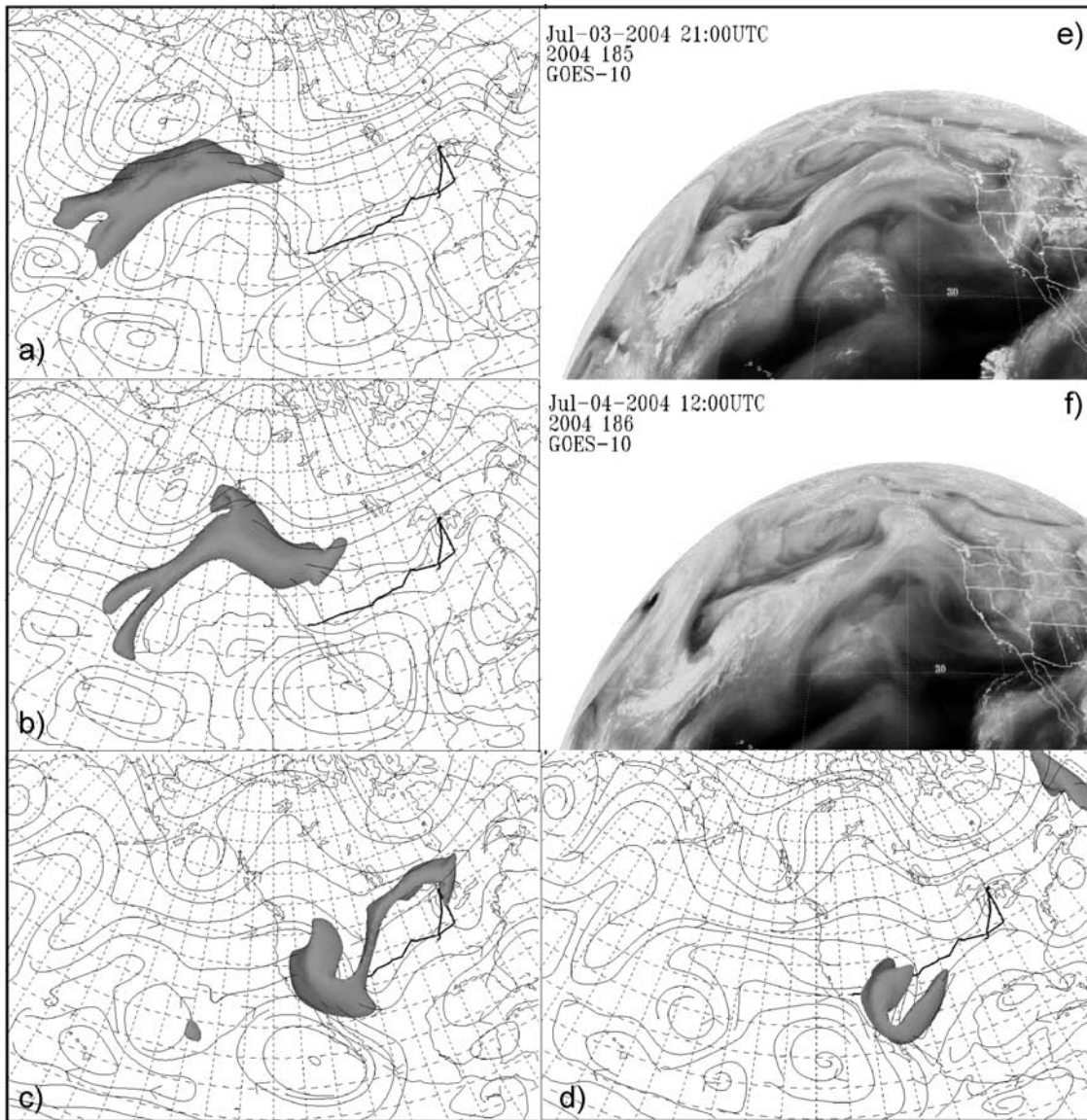


Figure 9. Progression of the 5 ppbv isosurface of SOC tracer at (a) 2100 UTC 3 July, (b) 1200 UTC 4 July, (c) 1900 UTC 5 July, and (d) 1600 UTC 6 July. GOES 10 water vapor images are shown for (e) 2100 UTC 3 July and (f) 1200 UTC 4 July. Note the “arcing dolphin” shape in both the isosurface and the convective outflow in the water vapor imagery. The isosurface encounters the split flow and separates into two segments by 6 July.

nearly under this structure. High values of convectively generated PV in the lower and middle troposphere are seen in the slice as well. Also shown is a green isosurface depicting where the SOC tracer value exceeds 40% of the background ozone value (recall that the SOC tracer is a measure of accumulated ozone flux). The tracer value is highest along the northern flank of the convectively modified region, although some higher values also appear near the ongoing convection, indicating some history of deeper mixing. The high percentage is attributable to both the strong downwelling surrounding the convection, and that background values are lower because of the convective dilution. (The values appearing right near the surface are likely due to a convectively induced lower tropospheric PV maximum and very low background values of ozone.) SOC

tracer can also be seen leaving the eastern boundary of the inner grid.

[23] Since the flux is only calculated every 20 min, this introduces some error in the value of the tracer. Given the integration of the calculation over 24 h, it is assumed that cancelation of spuriously high instantaneous flux values at any given time will allow for a reasonable first-order quantification. Figure 7b shows the total tendency of “SOC molecules” with time for the inner grid. For the first 18 h downward ozone transport increased SOC in the inner grid. Thereafter, a decreasing trend in SOC is seen as SOC tracer is advected eastward out of the inner domain.

3.3.2. Outer Grid: 3–6 July

[24] Figures 9a–9d show the evolution of the 5 ppbv SOC isosurface as it is transported across the Pacific. The

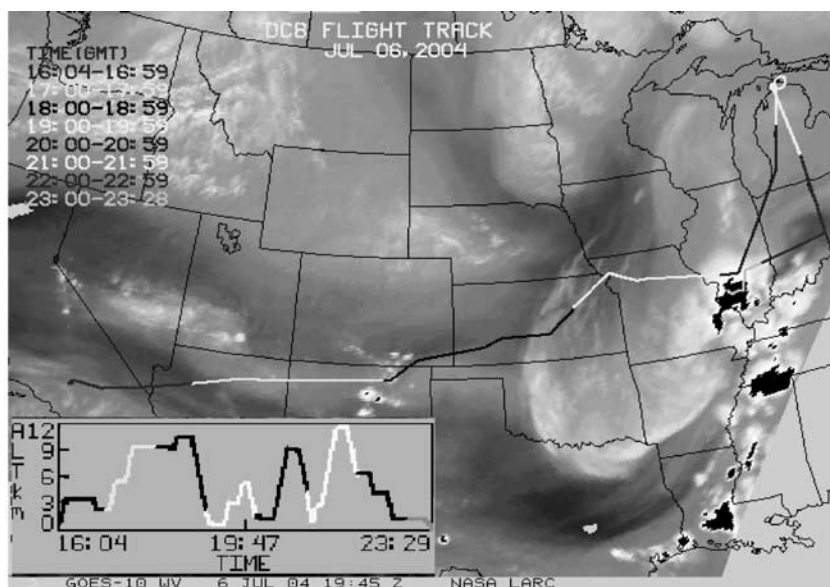


Figure 10. Horizontal projection of DC8 INTEX-NA flight 4 during 1605 to 2328 UTC 6 July 2004, superimposed on water vapor imagery from GOES 10 at 1945 UTC. Shaded segments delineate the time (top left) and altitude (bottom left) of the DC-8 during the flight.

tracer is drawn out zonally along the jet axis, with the bulk traveling northeast over the top of the upper level ridge. A “forked tail” develops on the southwestern end of the isosurface as a result of convective dilution of the tracer. The convective outflow is readily seen on GOES 10 water vapor imagery (Figures 9e and 9f). The tracer is advected over North America, with one main portion settling over the southwestern United States and northern Mexico, and the other streaming across the U.S.-Canadian border. By flight time (1600 UTC 6 July), a small but significant amount of SOC was positioned over the beginning portion of the flight track (Figure 9d). The portion of SOC over the southwestern United States lingered for several days past 6 July when the simulation was allowed to progress further, indicating a region of stagnant air.

4. Data Comparison and Results

4.1. Flight 4 Goals and Observations

[25] Flight 4 of the INTEX-NA campaign was a transit flight from Dryden Flight Research Center, California to Mid-America Airport, Illinois. Figure 10 shows a detailed plan view of the flight track along with the height of each flight segment in the lower left corner. Science objectives of INTEX-NA included identifying boundary layer pollution from California and fires over Arizona, analyzing convective outflow over the Midwest, as well as observing frontal structures and boundary layer pollution over the Ohio Valley. Another objective was to characterize upper tropospheric import from Asia. Over the beginning stages of the flight, elevated boundary layer pollution was noted, with sources from California and fires over Colorado and Arizona. Farther to the east, an ascent into the upper troposphere found weak pollution signatures, surmised to be from both Asia and the United States. Widespread convection over the central United States forced some

changes in the flight plan. Pollution plumes were sampled in the middle and upper troposphere. The flight passed through a cold front just before the northward turn near St. Louis (MO), along an upper tropospheric leg to near Sault Sainte Marie (MI), followed by a descent to St. Louis. Cloudiness forced an ascent before a step down through the troposphere back to Mid America Airport (near St. Louis); aerosols and nitric acid were prevalent along with low ozone levels in the boundary layer leg east of St. Louis.

[26] Figure 11a shows a curtain profile of UWNMS ozone along an interpolated flight track, while Figure 11b shows observed lidar data on flight 4. It is evident there are some discrepancies in the values of ozone in some regions, but much of the structure is well correlated. Since the simulation does not have a full chemistry package, lower tropospheric ozone values will tend to have more error, as source regions near the surface will dominate the variability. Interpolation errors of UWNMS values to the flight track also can contribute to the discrepancies. The main features in the lidar curtain profile are captured, such as the shape of the ozonopause, the relative maximum of ozone between 9 and 13 km during 2100–2200 UT, and the middle and upper tropospheric values of ozone observed by lidar generally agree with modeled values.

[27] Figure 12 shows a three-dimensional representation of the flight track, along with a vertical cross section of modeled ozone, and an isosurface representing SOC values exceeding 5% of the background ozone value. Figure 12 also shows how much of the flight path just missed the bulk of the SOC tracer, with the isosurface seeming to “curl around” the flight path. A curtain profile of SOC tracer, in percentage of background model ozone, are shown in Figure 13. Values exceeding 8% are shown near the tropopause (about 15 km) during the beginning portion of the flight. The original flight plan called for an earlier (by about an hour) ascent to the upper troposphere. It would

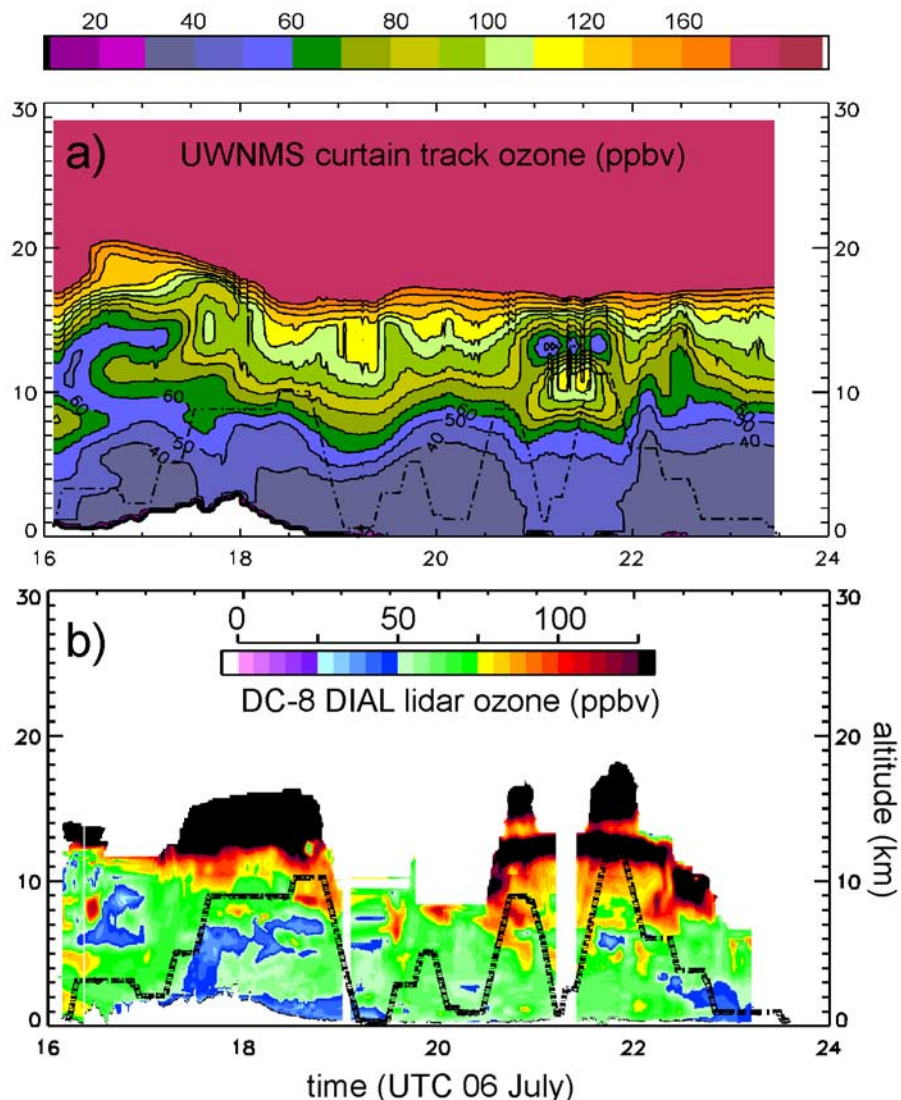


Figure 11. Comparison of interpolated UWNMS ozone with DC-8 DIAL lidar ozone for INTEX flight 4. (a) Curtain profile of interpolated UWNMS ozone along the flight and flight altitude (dashed line). (b) DC-8 DIAL lidar ozone and flight altitude (dashed line).

have been interesting to see more of the ozone structure at higher altitudes earlier in the flight, as this would have captured more of the region where the SOC was most prevalent.

[28] Although the values of SOC are quite small compared to the background ozone field, it is somewhat surprising that a significant percentage of ozone can be directly attributed to a 1-day source more than 5000 km distant. One might expect a more diffusive distribution of the SOC in cases where the jet stream is not so confined. Given that these types of convective systems occur quite regularly over the central Pacific, one must conclude that convectively induced SOC plays a large role in tropospheric ozone over North America, as well as the global stratospheric and tropospheric ozone budgets. Assuming there are three convective complexes similar to this study on any given day across the North Pacific, an estimate of the total

SOC for the summer season, from just convective ozone STE, yields about 50 Tg of ozone.

4.2. Coincident Studies

[29] *Al-Saadi et al.* [2005] analyzed long-range transport for the entire INTEX campaign using a Lagrangian source-receptor scheme. They found that midlatitude, upper tropospheric air over the INTEX region had a high correlation with sources near the tropopause over the subtropical and midlatitude Pacific when looking at time scales of 4 to 7 days. They also found this air to be characterized by strong Lagrangian mixing and elevated stratospheric influence. Our study focusing on a singular event of long-range transport corroborates well with these findings. The settling of SOC into the ridge over the southwestern United States (which persisted well beyond 6 July) is also consistent with the findings of AS2005, with upper tropospheric air over

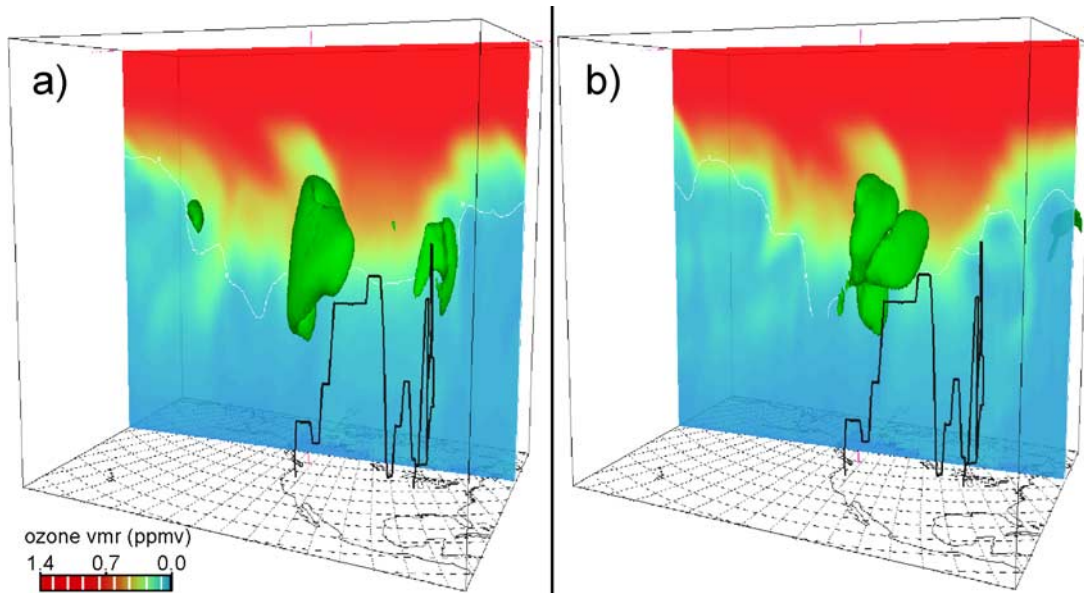


Figure 12. Vertical cross section of ozone (colored/shaded), the 1.3 PVU contour (white) across the outer domain, isosurface where SOC exceeds 5% of the background value of ozone, and the path of INTEX flight 4, for (a) 2200 UT 5 July and (b) 1700 UT 6 July.

North America having a local source in the upper troposphere at timescales of up to 10 days. This would seem to indicate a prevalence of upper tropospheric stagnation.

5. Conclusions

[30] Aircraft observations of ozone on the INTEX-NA transit flight of 6 July 2004 intersected a region influenced by long-range transport of SOC from a convective complex

over the central Pacific 3 days before. The UWNMS, initialized with RAQMS ozone fields, provided qualitative and quantitative pictures of the influence of this convection on tropospheric ozone over the INTEX-NA region. A two-scale method was used to determine the SOC in the region of convection within a nested grid, with a tracer representation of this ozone allowed to advect into the larger domain. Our analysis indicates that only 1 day of convection yielded about 0.2 Tg of SOC, which was quickly

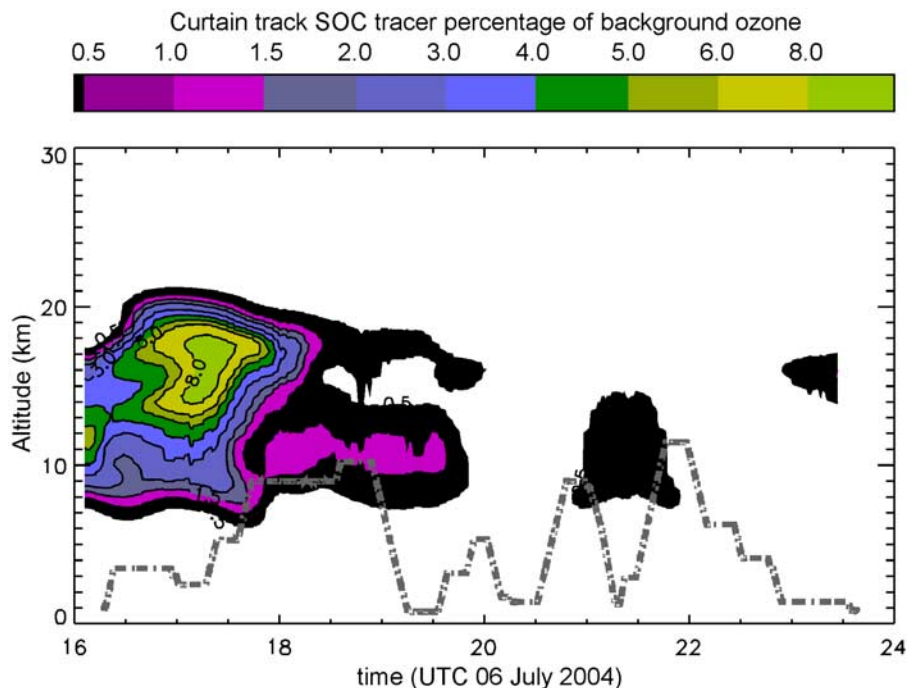


Figure 13. Curtain profile of SOC tracer as a percentage of background ozone along the flight track in the UWNMS. Values exceeded 8% at altitudes above the early portion of the flight.

advected across the Pacific and over North America by a convectively enhanced jet streak. Tracer values nearing 10% of the total ozone field were simulated over the southwestern United States 3 days later. We also found that, since the SOC tends to be near (or mixed with) convective outflow, the percentage of SOC was higher given the typical dilution of ozone in the core of the MCS. Tropospheric observations of “stratospheric influence” (such as ozone) are typically correlated with low water vapor. This particular case shows that convectively induced SOC would likely not have a strong anticorrelation with water vapor. Our findings are also in agreement with longer-term attribution studies showing a strong correlation of convectively mixed and stratosphere-influenced air in the upper troposphere over North America with sources over the central Pacific near the tropopause for synoptic timescales. Given the climatology of similar convective systems over the central Pacific, we conclude that the convectively enhanced SOC and its long-range transport make an important quantitative contribution to ozone over the United States.

[31] **Acknowledgments.** We thank the INTEX science team for their careful measurements, planning, and analysis which made this work possible. We thank Amanda Kis for obtaining and archiving satellite data for this study. We gratefully acknowledge support from NASA TRACE-P grant NCC1-01-011 and ACMAP grant NAG5-11303.

References

- Alexander, M., J. Holton, and D. Durran (1995), The gravity wave response above deep convection in a squall line simulation, *J. Atmos. Sci.*, *52*, 2212–2226.
- Al-Saadi, J., et al. (2005), Lagrangian characterization of the sources and chemical transformation of air masses observed by the NASA DC-8 during ICARTT/INTEX-A, *Eos Trans. AGU*, *86*(52), Fall Meet. Suppl., Abstract A53D-04.
- Barnes, S. L. (1973), Mesoscale objective map analysis using weighted time-series observations, *NOAA Tech. Memo. ERL NSSL-69*, 60 pp., Natl. Severe Storms Lab., Norman, Okla.
- Bluestein, H. (1993), *Synoptic-Dynamic Meteorology in Midlatitudes*, vol. II, 594 pp., Oxford Univ. Press, New York.
- Büker, M. L., M. H. Hitchman, G. J. Tripoli, R. B. Pierce, E. V. Browell, and M. A. Avery (2005), Resolution dependence of cross-tropopause ozone transport over east Asia, *J. Geophys. Res.*, *110*, D03107, doi:10.1029/2004JD004739.
- Ebel, A., et al. (1991), Simulation of ozone intrusion caused by a tropopause fold and cut-off low, *Atmos. Environ., Part A*, *25*(10), 2131–2144.
- Eckman, R. S., W. L. Grose, R. E. Turner, W. T. Blackshear, J. M. Russell III, L. Froidevaux, J. W. Waters, J. B. Kumer, and A. E. Roche (1995), Stratospheric trace constituents simulated by a three-dimensional general circulation model: Comparison with UARS data, *J. Geophys. Res.*, *100*, 13,951–13,966.
- Fritsch, J. M., and R. A. Maddox (1981), Convectively driven mesoscale weather systems aloft Part II: Numerical simulations, *J. Appl. Meteorol.*, *20*, 20–26.
- Gray, S. L. (2003), A case study of stratosphere to troposphere transport: The role of convective transport and the sensitivity to model resolution, *J. Geophys. Res.*, *108*(D18), 4590, doi:10.1029/2002JD003317.
- Haltiner, G. J., and R. T. Williams (1980), *Numerical Prediction and Dynamical Meteorology*, 2nd ed., John Wiley, New York.
- Hibbard, W. L., B. E. Paul, D. A. Santek, C. R. Dyer, A. L. Battaiola, and M. Voidrot-Martinez (1994), Interactive visualization of Earth and space science computations, *IEEE Comput.*, *27*(7), 65–72.
- Hitchman, M. H., and A. S. Huesmann (2007), A seasonal climatology of Rossby wave breaking in the layer 330–2000 K, *J. Atmos. Sci.*, *64*, 1922–1940.
- Hitchman, M. H., M. L. Büker, and G. J. Tripoli (1999), Influence of synoptic waves on column ozone during Arctic summer 1997, *J. Geophys. Res.*, *104*, 26,547–26,563.
- Hitchman, M. H., M. L. Buker, G. J. Tripoli, E. V. Browell, W. B. Grant, T. J. McGee, and J. F. Burris (2003), Nonorographic generation of Arctic polar stratospheric clouds during December 1999, *J. Geophys. Res.*, *108*(D5), 8325, doi:10.1029/2001JD001034.
- Hitchman, M. H., M. L. Buker, G. J. Tripoli, R. B. Pierce, J. A. Al-Saadi, E. V. Browell, and M. A. Avery (2004), A modeling study of an east Asian convective complex during March 2001, *J. Geophys. Res.*, *109*, D15S14, doi:10.1029/2003JD004312.
- Holton, J. R. (1992), *An Introduction to Dynamic Meteorology*, 3rd ed., Academic, San Diego, Calif.
- Hoskins, B. J., M. E. McIntyre, and A. W. Robertson (1985), On the use and significance of isentropic potential vorticity maps, *Q.J.R. Meteorol. Soc.*, *111*, 877–946.
- Johnson, D. R., T. H. Zapotocny, F. M. Reames, B. J. Wolf, and R. B. Pierce (1993), A comparison of simulated precipitation by hybrid isentropic sigma and sigma models, *Mon. Weather Rev.*, *121*, 2088–2114.
- Lamarque, J. F., and P. G. Hess (1994), Cross-tropopause mass exchange and potential vorticity budget in a simulated tropopause folding, *J. Atmos. Sci.*, *51*(15), 2246–2269.
- Maddox, R. A. (1980), An objective technique for separating macroscale and mesoscale features in meteorological data, *Mon. Weather Rev.*, *108*, 1108–1121.
- Mecikalski, J. R., and G. J. Tripoli (1998), Inertial available kinetic energy and the dynamics of tropical plume formation, *Mon. Weather Rev.*, *126*(8), 2200–2216.
- Mecikalski, J. R., and G. J. Tripoli (2003), Influence of upper-tropospheric inertial stability on the convective transport of momentum, *Q.J.R. Meteorol. Soc.*, *129*(590), 1537–1563.
- Pierce, R. B., et al. (2003), Regional air quality modeling system (RAQMS) predictions of the tropospheric ozone budget over east Asia, *J. Geophys. Res.*, *108*(D21), 8825, doi:10.1029/2002JD003176.
- Pierce, R. B., et al. (2007), Chemical data assimilation estimates of continental U.S. ozone and nitrogen budgets during the Intercontinental Chemical Transport Experiment North America, *J. Geophys. Res.*, *112*, D12S21, doi:10.1029/2006JD007722.
- Postel, G. A., and M. H. Hitchman (1999), A climatology of Rossby wave breaking along the subtropical tropopause, *J. Atmos. Sci.*, *56*, 359–373.
- Postel, G. A., and M. H. Hitchman (2001), A case study of Rossby wave breaking along the subtropical tropopause, *Mon. Weather Rev.*, *129*, 2555–2569.
- Pouliida, O., R. Dickerson, and A. Heymsfield (1996), Stratosphere-troposphere exchange in a midlatitude mesoscale convective complex: 1. Observations, *J. Geophys. Res.*, *101*(D3), 6823–6836, doi:10.1029/95JD03523.
- Sigmond, M., J. Meloan, and P. Siegmund (2000), Stratosphere-troposphere exchange in an extratropical cyclone, calculated with a Lagrangian method, *Ann. Geophys. Atmos.*, *18*(5), 573–582.
- Singh, H. B., W. H. Brune, J. H. Crawford, D. J. Jacob, and P. B. Russell (2006), Overview of the summer 2004 Intercontinental Chemical Transport Experiment North America (INTEX-A), *J. Geophys. Res.*, *111*, D24S01, doi:10.1029/2006JD007905.
- Stokes, G. G. (1847), On the theory of oscillatory waves, *Trans. Cambridge Philos. Soc.*, *8*, 441–455.
- Thorncroft, C. D., B. J. Hoskins, and M. E. McIntyre (1993), Two paradigms of baroclinic life-cycle behavior, *Q.J.R. Meteorol. Soc.*, *119*, 17–55.
- Tripoli, G. J. (1992), A nonhydrostatic numerical model designed to simulate scale interaction, *Mon. Weather Rev.*, *120*, 1342–1359.
- Waugh, D. W., and B. M. Funatsu (2003), Intrusions into the tropical upper troposphere: Three-dimensional structure and accompanying ozone and OLR distributions, *J. Atmos. Sci.*, *60*(4), 637–653.
- Wei, M. Y. (1987), A new formulation of the exchange of mass and trace constituents between the stratosphere and troposphere, *J. Atmos. Sci.*, *44*(20), 3079–3086.
- Wirth, V., and J. Egger (1999), Diagnosing extratropical synoptic-scale stratosphere-troposphere exchange: A case study, *Q.J.R. Meteorol. Soc.*, *125*, 635–655.
- Wu, R. G., and B. Wang (2000), Interannual variability of summer monsoon onset over the western North Pacific and the underlying processes, *J. Clim.*, *13*(14), 2483–2501.

J. A. Al-Saadi, E. V. Browell, and R. B. Pierce, NASA Langley Research Center, Hampton, VA 23681, USA. (jaal-saadi@larc.nasa.gov; e.v.browell@larc.nasa.gov; r.b.pierce@larc.nasa.gov)

M. L. Büker, M. H. Hitchman, and G. J. Tripoli, Department of Atmospheric and Oceanic Sciences, University of Wisconsin-Madison, 1225 W. Dayton, Madison, WI 53706, USA. (bukerm@uwosh.edu; matt@aos.wisc.edu; tripoli@aos.wisc.edu)